

Adaptive Hardness-driven Augmentation and Alignment Strategies for Multi-Source Domain Adaptations

Yuxiang Yang, Xinyi Zeng, Pinxian Zeng, Chen Zu, Binyu Yan, Jiliu Zhou, *Senior Member, IEEE*, and Yan Wang*, *Member, IEEE*

Abstract—Multi-source Domain Adaptation (MDA) aims to transfer knowledge from multiple labeled source domains to an unlabeled target domain. Nevertheless, traditional methods primarily focus on achieving inter-domain alignment through sample-level constraints, such as Maximum Mean Discrepancy (MMD), neglecting three pivotal aspects: 1) the potential of data augmentation, 2) the significance of intra-domain alignment, and 3) the design of cluster-level constraints. In this paper, we introduce a novel hardness-driven strategy for MDA tasks, named A^3 MDA, which collectively considers these three aspects through Addaptive hardness quantification and utilization in both data Augmentation and domain Alignment. To achieve this, A^3 MDA progressively proposes three Adaptive Hardness Measurements (AHM), i.e., Basic, Smooth, and Comparative AHMs, each incorporating distinct mechanisms for diverse scenarios. Specifically, Basic AHM aims to gauge the instantaneous hardness for each source/target sample. Then, hardness values measured by Smooth AHM will adaptively adjust the intensity level of strong data augmentation to maintain compatibility with the model’s generalization capacity. In contrast, Comparative AHM is designed to facilitate cluster-level constraints. By leveraging hardness values as sample-specific weights, the traditional MMD is enhanced into a weighted-clustered variant, strengthening the robustness and precision of inter-domain alignment. As for the often-neglected intra-domain alignment, we adaptively construct a pseudo-contrastive matrix by selecting harder samples based on the hardness rankings, enhancing the quality of pseudo-labels, and shaping a well-clustered target feature space. Experiments on multiple MDA benchmarks show that A^3 MDA outperforms other methods.

Index Terms—Multi-Source Domain Adaptation, Hardness-driven Augmentation and Alignment, Adaptive Hardness Quantification and Utilization.

This work is supported by National Natural Science Foundation of China (NSFC 62371325, 62071314), Sichuan Science and Technology Program 2023YFG0263, 2023YFG0025, 2023NSFSC0497, and Opening Foundation of Agile and Intelligent Computing Key Laboratory of Sichuan Province. The associate editor coordinating the review of this manuscript and approving it for publication was ***. (Corresponding author: Yan Wang)

Yuxiang Yang, Xinyi Zeng, Pinxian Zeng, Binyu Yan, Jiliu Zhou and Yan Wang are with School of Computer Science, Sichuan University, Chengdu, China. (e-mail: yangyuxiang3@stu.scu.edu.cn; perperstudy@gmail.com; 651215874@qq.com; yanbinyu2023@163.com; zhoujiliu@cuit.edu.cn; wangyanscu@hotmail.com).

Chen Zu is with JD.com. (e-mail: chen0zu@gmail.com)

Yuxiang Yang and Xinyi Zeng have equal contributions to this work.

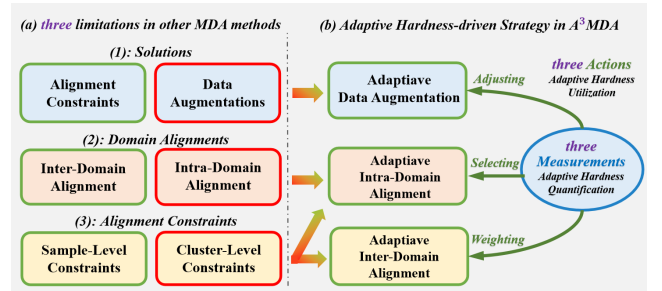


Fig. 1. Red boxes indicate aspects that are not covered or not handled effectively, while green boxes signify effectively handled aspects. The core idea of A^3 MDA lies in harnessing *three-fold* Adaptive hardness quantification and utilization to address *three* limitations.

I. INTRODUCTION

Unsupervised Domain Adaptation (UDA) has emerged as a crucial approach for aligning distributions between labeled data (source domain) and unlabeled data (target domain). This adaptation process can be categorized into two main types, namely, Single-source Domain Adaptation (SDA) [1]-[3] and Multi-source Domain Adaptation (MDA) [4]-[6]. SDA aims to learn the underlying relationships between a single labeled source domain and an unlabeled target domain to classify the target samples accurately. However, in practical applications, labeled source data can be collected from multiple domains. Consequently, compared to SDA, MDA has garnered significant attention as a more complex and realistic scenario [7]-[10].

Despite the promising performance, most MDA studies still encounter limitations at three levels, as shown in Fig. 1(a). Firstly, prevailing approaches predominantly emphasize alignment constraints (or modules) for solutions, such as adversarial discriminator [11], correlation alignment [12], and Maximum Mean Discrepancy (MMD) [13], [14], while ignoring the potential benefits of data augmentation. This preference for alignment over augmentation is rooted in apprehensions that standard augmentation techniques in current data-driven methods [15], whether fixed or random, may *inevitably over-augment hard samples, making them even harder to train and potentially exceeding the model’s generalization capability* [16]. Secondly, most MDA studies

only address the inter-domain shift by aligning multiple source domains and a target domain into a domain-invariant feature space [5], [17]. However, they often overlook the intra-domain shifts originating from latent noise within the unlabeled target domain. *These shifts, especially noticeable in **hard target samples** near the decision boundary, can substantially undermine the categorizability of the target feature space.* In the MDA setting, such hard samples often exhibit increased uncertainty, posing challenges to a robust alignment process. Thirdly, conventional discrepancy-based methods typically employ plain constraints, such as MMD, to perform domain alignments at the sample level [18], [19]. In other words, the designed constraints indiscriminately reduce the differences between samples across domains at a coarse level, without taking into account sample-specific attributes for adaptive utilization. These attributes, including (pseudo/real)-class labels indicating their cluster memberships, and the ***hardness values*** like entropy [20]-[22] and confidence [23], [24] *that can signify their levels of learning difficulty and classification uncertainty, have the potential to enhance domain alignment with greater precision and robustness.*

Motivated to address this tripartite limitation, we propose a novel hardness-driven strategy, named A³MDA, for MDA classification tasks. As shown in Fig. 1(b), all designs involving data Augmentation and domain Alignment are Adaptively guided by the quantification and utilization of sample-specific hardness throughout training. To achieve this, we devise three progressive Adaptive Hardness Measurements (AHM), i.e., Basic, Smooth, and Comparative AHMs. Concretely, Basic AHM is designed to gauge the difficulty of each sample and is then refined into a Smooth AHM through a historical smoothing mechanism to mitigate random fluctuations that could disrupt instantaneous hardness assessments. The hardness values from Smooth AHM are adaptively employed to adjust the intensity levels of strong data augmentations, ensuring compatibility with the model’s generalization capacity. Based on Smooth AHM, Comparative AHM introduces a comparison mechanism by comparing hardness values among samples within a batch or batch-wise cluster, thereby dynamically adjusting the inter- and intra-domain alignment within cluster-level constraints. Specifically, for inter-domain alignment, the hardness values from Comparative AHM serve as sample-specific weights, in conjunction with class attributes, to enhance the traditional MMD loss into a weighted-clustered variant. This modification greatly bolsters the robustness and precision in aligning source and target distributions. As for the often-overlooked intra-domain alignment, instead of directly weighting hard samples in the loss function, we utilize their hardness rankings to adaptively select harder samples to form a pseudo-contrastive matrix. By incorporating it as an integral optimization component, A³MDA greatly improves the quality of pseudo labels and the categorizability of the target feature space. Our contributions are:

- 1) We introduce a novel hardness-driven strategy, A³MDA, centered on a *three*-fold adaptive hardness quantification

and utilization to tackle *three* limitations in MDA classification tasks. Experiments on various benchmarks demonstrate its effectiveness and generalizability.

- 2) For adaptive hardness quantification, A³MDA employs *three* progressive Adaptive Hardness Modules (AHMs) - Basic, Smooth, and Comparative. Each progression incorporates unique mechanisms tailored to diverse augmentation and alignment scenarios.
- 3) For adaptive hardness utilization, we implement *three* actions: (a) We utilize Smooth AHM to adaptively guide the intensity of data augmentation, preventing over-augmentation and aligning with evolving generalization capabilities. (b) We leverage values from the Comparative AHM as sample-specific weights, transforming traditional MMD into a weighted-clustered variant to enhance the robustness and precision of inter-domain alignment. (c) We develop a pseudo-contrastive matrix based on selected harder samples for the often-neglected intra-domain alignment, which effectively eliminates erroneous pseudo-labels and shapes a well-clustered feature space.

II. RELATED WORK

A. SDA and MDA methods

Single-source Domain Adaptation (SDA) aims to transfer knowledge from a labeled source domain to an unlabeled target domain. SDA methods can be categorized into adversarial- and discrepancy-based methods. Adversarial-based methods [2], [4], [25], [26] focus on reducing the data distribution gap between the source and target domains by employing adversarial discriminators. On the other hand, discrepancy-based methods primarily utilize correlation learning or divergence learning to align source and target domains. Correlation learning focuses on directly minimizing differences in feature covariances between source and target domains [54-56], [70]. For example, Lu et al. [54] proposed a method that integrates graph embedding and sample reweighting to learn weighted correlation embeddings. In contrast, divergence losses, particularly Maximum Mean Discrepancy (MMD) and its variants, have been widely studied [13], [27]-[28] to minimize the distance between the distributions of domains in a reproducing kernel Hilbert space. Recent advancements in SDA include innovative approaches like optimal transport [57], graph learning [71], and flexible strategies such as test-time adaptation [59]. Besides traditional classification tasks, SDA has also been applied to various other domains. For example, Nguyen et al. [58] proposed a cross-domain kernel classifier and applied the max-margin principle to enhance software vulnerability detection.

In real-world scenarios characterized by diverse and complex source distributions, SDA methods often fall short of achieving competitive performance. Recently, Multi-source Domain Adaptation (MDA) methods have emerged to expand upon traditional SDA techniques, aiming to tackle more practical scenarios in which labeled training samples are gathered from multiple sources. For instance, STEM [29], a well-designed adversarial-guided method, employs a teacher-

student architecture that provides robust theoretical guarantees regarding each component’s role in domain transfer. Despite its impressive performance, STEM inevitably involves training an additional source-domain discriminator to assist the teacher expert, along with a student adversarial discriminator to minimize the gap between the mixture of source domain distributions and the target distribution. In contrast, MFSAN [18], a typical streamlined discrepancy-based method, relies solely on MMD without introducing additional modules for domain alignment and generates target predictions based on source-specific modules directly. Despite its effectiveness, the method does not fully consider sample attributes (e.g. sample hardness and class attributes) when applying MMD constraint, as normal and hard samples are treated equally. Moreover, like most other discrepancy-based MDA classification methods, it does not address intra-domain alignment. The core idea for this issue is to enhance inter-class separability and intra-class compactness by clustering similar target samples together while pushing dissimilar samples apart. However, despite the growing focus on reducing the intra-domain gap in other research areas [60], [61], many existing unsupervised MDA methods tend to overlook this aspect, posing challenges in shaping a well-clustered feature space to achieve further improvements in the target domain.

B. Hardness and Uncertainty-based Measurements

Recently, hardness or uncertainty has gradually emerged as an extra focus for hard sample mining [21], [30] and curriculum learning [31]. For instance, some works [20], [21] leverage the entropy values of target predictions as an uncertainty measurement and minimize them to facilitate domain transfer. Similarly, some other studies [32], [33] endeavor to employ entropy-based hardness analysis on all unlabeled target samples, ranking and categorizing them into hard and easy groups based on a predefined threshold. Furthermore, some recent research has addressed uncertainty regarding label-wise and pair-wise correspondence in other fields, exploring the implications of noisy labels [62]-[64]. For instance, Yang et al. [62] proposed a novel method addressing coupled noisy labels in object Re-ID, effectively rectifying annotation errors. Lin Y. et al. [63] proposed a contrastive matching with momentum distillation for addressing bi-level noisy correspondence in graph matching.

However, most hardness-driven methods in MDA classification tasks primarily rely on direct and instantaneous *entropy measurement*, lacking the involvement of *class attributes (label information)* and *specialized designs (mechanisms)* for diverse scenarios. Such reliance severely restricts the applicability and generalizability of evaluated hardness values. Consequently, despite a few works [34], [35] using model-adaptive hardness strategies in other tasks, most MDA methods only engage sample hardness for qualitative selecting purposes, leaving quantitative hardness applications largely unexplored. As shown in Fig. 1(b), A³MDA addresses the tripartite limitation in MDA with progressive AHMs, with each progress injecting distinct mechanisms to apply hardness values to all given augmentation and alignment scenarios.

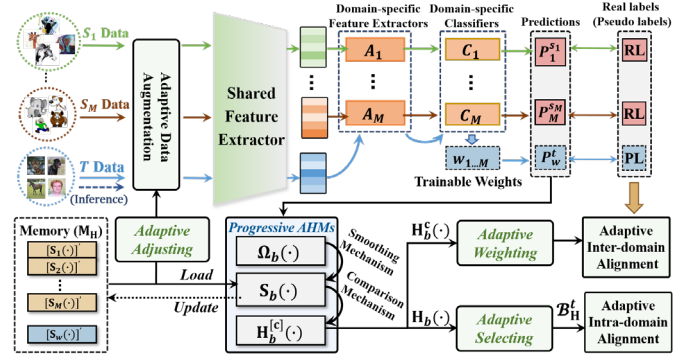


Fig. 2. Diagram of our A³MDA framework. Consistent with Fig. 1, **Adaptive Hardness Quantification** derives hardness values from *three* progressive measurements (Basic, Smooth, and Comparative AHM). **Adaptive Hardness Utilization** adaptively leverages them across three scenarios through *three* types of actions (adjusting for data augmentation, weighting for inter-domain alignment, selecting for intra-domain alignment).

III. METHODOLOGY

MDA aims to transfer knowledge from M labeled source domains $\{S_m\}_{m=1}^M$ to one unlabeled target domain T . This corresponds to the m -th source batch $\mathcal{B}^{sm} = \{x_i^{sm}, y_i^{sm}\}_{i=1}^{|\mathcal{B}^{sm}|}$ and target batch $\mathcal{B}^t = \{x_i^t\}_{i=1}^{|\mathcal{B}^t|}$ ($|\mathcal{B}^{sm}| = |\mathcal{B}^t|$) during training. x_i^{sm} represents the i -th labeled source image and $RL = y_i^{sm} \in \{0,1\}^K$ denotes its one-hot real label, where K is the number of classes. x_i^t represents the i -th unlabeled target image.

As shown in Fig. 2, the architecture of A³MDA comprises a shared CNN-based feature extractor $F(\cdot)$, followed by M domain-specific feature extractors $\{A_m(\cdot)\}_{m=1}^M$ and classifiers $\{C_m(\cdot)\}_{m=1}^M$. After retrieving smoothed hardness values from the hardness memory (M_H), each x_i^{sm} and x_i^t will undergo adaptive augmentation and be fed into $F(\cdot)$ to generate features F_i^{sm} and F_i^t . The source feature F_i^{sm} is then fed into its own (m -th) domain-specific modules $A_m(\cdot)$ and $C_m(\cdot)$, producing the aligned feature $F_{m,i}^{sm}$ and prediction $P_{m,i}^{sm}$, while the target feature F_i^t is processed by $A_m(\cdot)$ and $C_m(\cdot)$ for every source domain, generating M features $F_{m,i}^t$ and predictions $P_{m,i}^t$. Notably, M predictions are further combined with trainable weights w_m to generate a weighted prediction $P_{w,i}^t = \sum_{m=1}^M w_m \cdot P_{m,i}^t$. For a target sample x_i^t , $P_{w,i}^t$ is also used to derive its one-hot pseudo-label $PL = \hat{y}_i^t = \text{onehot}(\text{argmax}(P_{w,i}^t)) \cdot 1(z_{\hat{a}} > \tau)$, where $z_{\hat{a}} = \max(P_{w,i}^t)$ is the confidence of the pseudo-class \hat{a} , and τ is the confidence threshold to select pseudo-labels.

A. Adaptive Hardness Quantification

Prevalent hardness-driven methods simply utilize entropy as a direct measure of hardness, interpreting samples with higher entropy values to have higher levels of difficulty (or uncertainty). Despite proving effectiveness in other unsupervised or supervised classification contexts, most methods solely measure the difficulty of samples at the current epoch and typically employ assessed values as qualitative

filters to select hard samples for further processing. Consequently, they struggle to effectively address the diverse scenarios encountered in Multi-source Domain Adaptation (MDA) tasks. To address this, we introduce a series of mechanisms to achieve the *Adaptive Hardness Quantification* for different scenarios. Specifically, we progressively propose *three Adaptive Hardness Measurements* (AHMs) to adaptively quantify the hardness of each labeled source and unlabeled target sample throughout training.

Basic AHM. Our progressive AHMs begin with a Basic version, denoted as $\Omega_b(\cdot)$, to gauge the instantaneous hardness in the current epoch. For any source or target sample x_i^a with its prediction $P_{b,i}^a$, $\Omega_b(x_i^a)$ is expressed as:

$$\Omega_b(x_i^a) = \sqrt{\sum_{j=1}^K ([P_{b,i}^a]_j)^2 \cdot (1 - \delta_{j,z})},$$

$$b = \begin{cases} m, a = s_m \\ w, a = t \end{cases}, z = \begin{cases} k, a = s_m \\ \hat{d}, a = t \end{cases}, \delta_{j,z} = \begin{cases} 1, j = z \\ 0, j \neq z \end{cases} \quad (1)$$

where a represents the domain in which the sample resides (s_m : m -th source or t : target). b denotes modules that generate predictions (m : domain-specific modules of m -th source $C_m(A_m(\cdot))$; w : passing all modules and weighting their outputs $\sum_{m=1}^M w_m \cdot C_m(A_m(\cdot))$). z represents the real class (index) k or the pseudo-class (index) \hat{d} . The Kronecker delta $\delta_{j,z}$ is used to ascertain whether index j matches the pseudo or real class index (z) of x_i^a . In simple terms, the role of Basic AHM is to set the element representing the real class (k) in $P_{m,i}^{s_m}$ and the pseudo-class (\hat{d} , also the element with the maximum value) in $P_{w,i}^t$ to 0, and then calculates the L2-norm of the remaining elements. To illustrate, for an m -th source domain sample $x_i^{s_m}$ with a prediction $P_{m,i}^{s_m} = [0.1 \ 0.1 \ 0.8]$ produced by domain-specific classifier $C_m(\cdot)$ and a true label $y_i^{s_m} = [0 \ 0 \ 1]$, the value of $\Omega_m(x_i^{s_m})$ is $\sqrt{(0.1)^2 + (0.1)^2}$, whereas for a more uncertain target sample x_i^t with the weighted prediction $P_{w,i}^t = [0.2 \ 0.3 \ 0.5]$, we have $\Omega_w(x_i^t) = \sqrt{(0.2)^2 + (0.3)^2} > \Omega_m(x_i^{s_m})$. This implies that more uncertain/harder samples have greater values in $\Omega_m(\cdot)$. Notably, x_i^t utilizes weighted predictions $P_{w,i}^t$ generated by all modules to enable comprehensive handling of target samples.

Smooth AHM. Basic AHM may cause instability due to random fluctuations since it only provides assessments of sample hardness in the current epoch. To mitigate this, we introduce Smooth AHM $\mathbf{S}_b(\cdot)$ based on $\Omega_b(\cdot)$, which employs Exponential Moving Average (EMA) for temporal smoothing of the evaluated hardness. The formula is:

$$\mathbf{S}_b(x_i^a) = \beta \cdot [\mathbf{S}_b(x_i^a)]' + (1 - \beta) \cdot \Omega_b(x_i^a), \quad (2)$$

where $[\mathbf{S}_b(x_i^a)]'$ represents the smoothed hardness values of x_i^a in the previous epoch (retrieved from memory \mathbf{M}_H), while $\mathbf{S}_b(x_i^a)$ represents the smoothed values of the current epoch. By giving a higher weight (smoothing factor β) to the previous $[\mathbf{S}_b(x_i^a)]'$ and lower weight to the current $\Omega_b(x_i^a)$, $\mathbf{S}_b(\cdot)$ focuses more on long-term trends and changes in sample hardness. Notably, \mathbf{M}_H will be also updated with the current $\mathbf{S}_b(x_i^a)$ to participate in the next training epoch.

Comparative AHM. Smooth AHM guarantees the stability

of evaluated hardness values. Nonetheless, this absolute stability might not be apt for alignment constraints that only involve batch-wise updates for optimization. This is because using the absolute hardness measure $\mathbf{S}_b(\cdot)$ in constraints can result in certain samples dominating or being marginalized within particular batches, thereby affecting the overall alignment process. To mitigate this concern, we introduce the Comparative AHM, which creates a competitive environment for assessing the relative hardness within each batch or batch-wise cluster. The formula is:

$$\mathbf{H}_b^{[c]}(x_i^a) = \frac{\mathbf{S}_b(x_i^a)}{\sum_{x_j^a \in \mathcal{B}_{[k/\hat{d}]}} \mathbf{S}_b(x_j^a)}, \quad (3)$$

where $[c]$ denotes the decision to introduce cluster-wise comparison alongside batch-wise comparison. When represented as the cluster-wise version $\mathbf{H}_b^c(\cdot)$, it indicates the selection of samples with the same real class (e.g., k) from the source batch \mathcal{B}^{s_m} or the same pseudo-class (e.g., \hat{d}) from the target batch \mathcal{B}^t . This selection creates the corresponding $\mathcal{B}_k^{s_m}$ and $\mathcal{B}_{\hat{d}}^t$ for dual-level comparisons. While in the default version $\mathbf{H}_b(\cdot)$, all samples from \mathcal{B}^{s_m} or \mathcal{B}^t are used.

The progressive design in AHMs embodies our pursuit of Adaptive Hardness Quantification, greatly extending the usability of the measured values. Therefore, our focus is not confined solely to qualitative analysis but also enables us to adaptively utilize hardness across various MDA scenarios.

B. Adaptive Hardness Utilization

With the acquired progressive hardness values, our attention shifts towards the adaptive utilization of the introduced mechanisms to align with the required properties for diverse MDA scenarios. This necessitates the selection of the most suitable AHM for estimation and adaptive structuring when implementing augmentation and constraints. Fundamentally, these AHMs exhibit an accordant positive correlation, with higher values indicating increased sample hardness and uncertainty. In A³MDA, our guideline of Adaptive Hardness Utilization is that: for harder samples, we should adaptively alleviate the intensity of data Augmentation while reinforcing the potency of domain Alignment. This guideline is realized through *three Actions - Adjusting, Weighting, and Selecting*.

Adaptive Data Augmentation - Adjusting. Existing MDA methods typically involve either randomly selecting or using a fixed set of predefined strong augmentations, which are then applied to weakly augmented samples. However, as highlighted in [16], using sample-agnostic strong augmentations can potentially disrupt data distributions in early training stages. Particularly in the MDA context, disregarding the diversity and learning difficulties can inevitably lead to excessive augmentation on already hard-to-train samples. Consequently, some methods [2], [36], despite the increased training burden, resort to augmentations using mutual techniques (e.g., Mixup [37] and CutMix [38]) or searching techniques (e.g., AutoAugment [39] or RandAugment [40]). In contrast, A³MDA continues to rely on

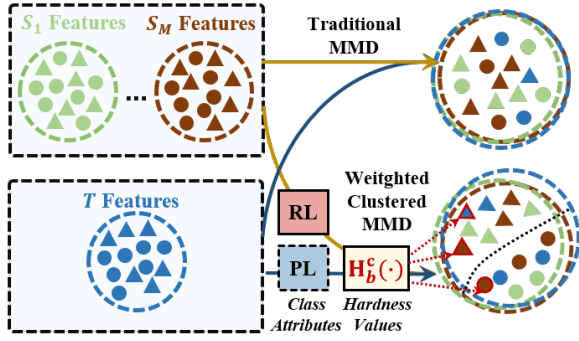


Fig. 3. Illustration of adaptive inter-domain alignment using hardness values from Comparative AHM as weights with class attributes to construct weighted-clustered MMD.

individual strong augmentations, but leverages smoothed hardness to adaptively modulate their intensity levels by:

$$\mathbf{h} = \begin{cases} [\mathbf{S}_m(x_i^{s_m})]', a = s_m \\ [\mathbf{S}_w(x_i^t)]', a = t \end{cases}$$

$$\mathcal{A}_{\mathcal{A}}(x_i^{s_m}) = \mathbf{h} \cdot \mathcal{A}_w(x_i^{s_m}) + (1 - \mathbf{h}) \cdot \mathcal{A}_s(x_i^{s_m}), \quad (4)$$

where the temporary variable \mathbf{h} denotes the hardness values (i.e. $[\mathbf{S}_m(x_i^{s_m})]'$ and $[\mathbf{S}_w(x_i^t)]'$) previously measured by Smooth AHM in Eq. (2), retrieved from the memory \mathbf{M}_H using the image indexes of $x_i^{s_m}$ and x_i^t . $\mathcal{A}_w(\cdot)$ represents weak augmentations, including random scaling, flipping, and cropping, and $\mathcal{A}_s(\cdot)$ encompasses intensity-based strong augmentations, such as invert, blur, contrast, and color jittering, etc., employing settings identical to [16]. We found that this categorization of strong and weak augmentations, beneficial for segmentation, also contributes positively to our application in the MDA classification with adaptive augmentation strategies. The final augmentation, denoted as $\mathcal{A}_{\mathcal{A}}(\cdot)$, adaptively adjusts the intensity level by scaling the proportions of $\mathcal{A}_s(\cdot)$ and its $\mathcal{A}_w(\cdot)$ counterpart. This method shields harder samples from excessive perturbation during early training stages, while also allowing easier, well-fitted samples to benefit from their strongly augmented versions as the model progresses. Notably, the introduced smoothing mechanism in $\mathbf{S}_b(\cdot)$ enables $\mathcal{A}_{\mathcal{A}}(\cdot)$ to progressively raise its intensity levels for various samples, thereby better adapting to the model's evolving generalization ability.

Adaptive Inter-domain Alignment - Weighting. A popular strategy in MDA is to minimize inter-domain shifts by imposing discrepancy-based constraints [5], [41], which involves utilizing metrics such as Maximum Mean Discrepancy (MMD) [13], [14] to measure the distance between the distributions of the source and target domains. The formula for traditional MMD loss is:

$$\mathcal{L}_{mmd} = \|\bar{\phi}_i^{s_m} - \bar{\phi}_i^t\|_{\mathcal{H}}^2,$$

$$\bar{\phi}^a = \frac{1}{|\mathcal{B}^a|} \sum_{i=1}^{|\mathcal{B}^a|} \phi_i^a, \quad (5)$$

where $\phi_i^{s_m}$ and ϕ_i^t are feature mappings from input samples $x_i^{s_m}$ and x_i^t to a reproducing kernel \mathcal{H} ilbert space. $\bar{\phi}^{s_m}$ and $\bar{\phi}^t$ denote their corresponding means.

Despite achieving satisfactory results in many cases, traditional MMD still exhibits limitations in MDA scenarios.

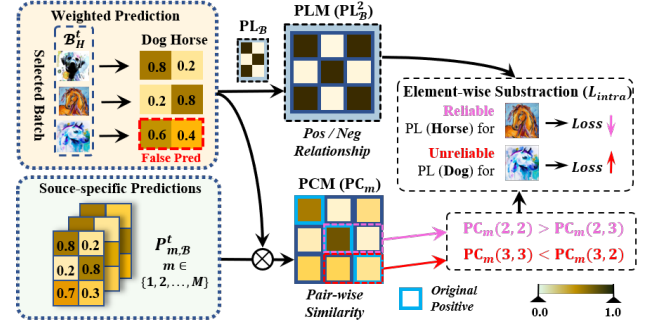


Fig. 4. Illustration of adaptive intra-domain alignment. Target batch \mathcal{B}_H^t is selected based on the sorting of Comparative AHM values. The intra-domain loss is then built by element-wise subtraction of PLM and PCM.

To clarify, we categorize it and similar constraints as ‘sample-level’, as they primarily achieve a coarse alignment between source and target distributions by pulling each source and target sample closer. However, such sample-level constraints indiscriminately average distances between each source and target sample, even when they belong to different classes. This imprecise alignment hinders accurate predictions.

To address these limitations, we introduce ‘cluster-level’ constraints, aiming to *achieve a finer alignment by adaptively fostering intra-class convergence while promoting inter-class divergence*. As shown in Fig. 3, we implement this constraint by combining \mathcal{L}_{mmd} with sample-specific attributes (category and hardness), resulting in a weighted-clustered variant \mathcal{L}_{mmd}^{WC} for adaptive inter-domain alignment. Specifically, class attributes use the real label $y_i^{s_m}$ with index k for the source sample $x_i^{s_m}$ and pseudo-label \hat{y}_i^t with index \hat{d} for target sample x_i^t . As for hardness values, unlike data augmentations that use Smooth AHM to gradually adjust the intensity level, we employ cluster-wise Comparative AHM $\mathbf{H}_b^c(\cdot)$ from Eq. (3) to adaptively evaluate the relative importance within batch-wise clusters, assigning greater weights to harder samples. The expression is:

$$\bar{\phi}_{\mathbf{H},k}^{s_m} = \frac{1}{|\mathcal{B}_k^{s_m}|} \sum_{i=1}^{|\mathcal{B}_k^{s_m}|} \phi_{\mathbf{H},i}^{s_m}, \phi_{\mathbf{S},i}^{s_m} = \mathbf{H}_m^c(x_i^{s_m}) \cdot \phi_i^{s_m},$$

$$\bar{\phi}_{\mathbf{H},\hat{d}}^t = \frac{1}{|\mathcal{B}_{\hat{d}}^t|} \sum_{i=1}^{|\mathcal{B}_{\hat{d}}^t|} \phi_{\mathbf{H},i}^t, \phi_{\mathbf{H},i}^t = \mathbf{H}_w^c(x_i^t) \cdot \phi_i^t, \quad (6)$$

$\mathcal{L}_{mmd}^{WC}(p^{s_m}, p^t) = \sum_{k=1}^{K_c} \left[\|\bar{\phi}_{\mathbf{H},k}^{s_m} - \bar{\phi}_{\mathbf{H},\hat{d}=k}^t\|_{\mathcal{H}}^2 - \|\bar{\phi}_{\mathbf{H},k}^{s_m} - \bar{\phi}_{\mathbf{H},\hat{d} \neq k}^t\|_{\mathcal{H}}^2 \right]$, where $\phi_i^{s_m}$ and ϕ_i^t are further enhanced to $\phi_{\mathbf{S},i}^{s_m}$ and $\phi_{\mathbf{H},i}^t$ by incorporating sample-specific weights generated by $\mathbf{H}_b^c(\cdot)$. The former term in \mathcal{L}_{mmd}^{WC} is to minimize when $x_i^{s_m}$ and x_i^t have the same category attributes $\hat{d} = k$, and the latter term is to maximize when $\hat{d} \neq k$. K_c represents the set of common classes between $\mathcal{B}_k^{s_m}$ and $\mathcal{B}_{\hat{d}}^t$.

With the dual-level comparisons in $\mathbf{H}_b^c(\cdot)$, \mathcal{L}_{mmd}^{WC} can automatically balance the batch-wise importance among different samples with the same class, thus enhancing the batch-based optimization. The final Inter loss combines \mathcal{L}_{mmd} and \mathcal{L}_{mmd}^{WC} for both coarse and fine inter-domain alignments:

$$\mathcal{L}_{Inter}(p^{s_m}, p^t) = (\mathcal{L}_{mmd} + \mathcal{L}_{mmd}^{WC})(p^{s_m}, p^t). \quad (7)$$

Algorithm 1 A³MDA algorithm in a mini-batch.

Input: Current Epoch (n), labeled source batch \mathcal{B}^{sm} , labeled target batch \mathcal{B}^t , Hardness Memory \mathbf{M}_H .

Parameters: Smoothing factor β , threshold τ , selection ratio R , Inter loss weight λ_1 , Intra loss weight λ_2 .

for $\{x_i^{sm}, y_i^{sm}\} \in \mathcal{B}^{sm}$ and $\{x_i^t\} \in \mathcal{B}^t$ **do**

Augment x_i^{sm}, x_i^t with M_H by Eq. (4).

Derive mapping for ϕ_i^{sm}, ϕ_i^t and predictions $P_{m,i}^{sm}, P_{m,i}^t$.

Derive weighted prediction $P_{w,i}^t$ and pseudo-label \hat{y}_i^t .

Calculate Basic AHM: $\Omega_m(x_i^{sm}), \Omega_w(x_i^t)$ by Eq. (1).

Calculate Smooth AHM: $\mathbf{S}_m(x_i^{sm}), \mathbf{S}_w(x_i^t)$ and update \mathbf{M}_H with β by Eq. (2).

end for

Calculate Comparative AHM: $\mathbf{H}_m^c(x_i^{sm}), \mathbf{H}_w^c(x_i^t), \mathbf{H}_w(x_i^t)$ by Eq. (3).

Create $\mathcal{B}_k^{sm}, \mathcal{B}_{\hat{a}=k}^t, \mathcal{B}_{\hat{a} \neq k}^t$ for each class k . Calculate \mathcal{L}_{Inter} by Eqs. (5) to (7).

Create \mathcal{B}_H^t by selecting with top ($R\%$) $\mathbf{H}_w(\cdot)$ values in \mathcal{B}^t . Calculate \mathcal{L}_{Intra} by Eqs. (8) to (9).

Calculate \mathcal{L}_{cls} using $\langle P_{m,i}^{sm}, y_i^{sm} \rangle$ and $\langle P_{w,i}^t, \hat{y}_i^t \rangle$.

return $\lambda_1 \cdot \mathcal{L}_{Inter} + \lambda_2 \cdot \mathcal{L}_{Intra} + \mathcal{L}_{cls}$ by Eq. (10).

Adaptive Intra-domain Alignment - Selecting. As highlighted in [32], [42], comprehensively predicting target labels based on a categorizable target feature space is crucial for enhancing performance. To achieve this, some methods [5], [6], [11], [43] utilize predictions from all domain-specific classifiers to generate a weighted prediction $P_{w,i}^t = \sum_{m=1}^M w_m \cdot P_{m,i}^t$, with trainable weights w_m dictate the reliance on various sources. Despite evident improvements over average predictions, such comprehensiveness remains vulnerable to challenges posed by the intra-domain shift. The intra-domain shift stems from the noise and inconsistencies within the target data distributions, particularly evidenced by certain hard samples that exhibit more resemblance to samples from other classes than their own. These hard samples can cause over-reliance on certain source domains in the weighted prediction, potentially leading to erroneous pseudo-labels and the distortion of the target feature space.

To reduce the intra-domain shift, A³MDA introduces another *cluster-level* constraint based on weighted predictions of hard samples. Similar to \mathcal{L}_{mmd}^{WC} , the constraint for intra-domain alignment also integrates a dual-level comparison mechanism, but is implemented in two operations: (1) an external batch-wise selection of harder samples using the rankings of default Comparative AHM $\mathbf{H}_b(\cdot)$, and (2) an internal cluster-wise competition using a pseudo-contrastive matrix. The rationale for not directly using the cluster-wise version $\mathbf{H}_b^c(\cdot)$ is that employing it as weights in a purely unsupervised constraint is unfeasible due to its dependence on relatively reliable pseudo-labels, and utilizing it to select harder samples may also yield an unstable prioritization, especially in batch-wise clusters with limited samples.

As shown in Fig. 4, the batch-wise selection of harder samples is achieved by sorting all target samples in batch \mathcal{B}^t based on their $\mathbf{H}_b(\cdot)$ (also $\mathbf{H}_w(\cdot)$) rankings, and retaining the top R (selection ratio) to form a new batch, denoted as \mathcal{B}_H^t .

Then, we create a Pseudo-Label Matrix (PLM) $\text{PL}_B^2 = \text{PL}_B \cdot \text{PL}_B^T$ to establish batch-wise positive/negative relationships, where $\text{PL}_B \in \mathbb{R}^{|\mathcal{B}_H^t| \times K}$ combines the pseudo-labels of all target samples in \mathcal{B}_H^t , and PL_B^T represents its transposition. Here, $(\text{PL}_B^2)_{i,j} = 1/0$ indicates whether the i -th and j -th samples in the target batch \mathcal{B}^t are positive (1: with the same pseudo-class) or negative (0: with different pseudo-class) pairs. For diagonal elements in PL_B^2 , their values are always 1, as each sample is positive with itself; for non-diagonal elements, their values depend on whether two samples share the same pseudo-class.

After establishing PLM, our attention turns to compute pairwise similarities by constructing diverse views of samples. This is achieved via a Pseudo Contrastive Matrix (PCM). In contrast to the traditional contrastive learning, which augments anchors to create a single positive view and projects these views into feature vectors, PCM directly selects weighted predictions as anchors and uses predictions with the same or different pseudo-classes, generated by domain-specific classifiers, as positive or negative views. The PCM for the m -th source is represented as:

$$(\text{PC}_m)_{i,j} = \frac{\exp(P_{w,i}^t \cdot P_{m,j}^t / \text{tem})}{\sum_{x_k^t \in \mathcal{B}_H^t} \exp(P_{w,i}^t \cdot P_{m,k}^t / \text{tem})}, \quad (8)$$

where $(\text{PC}_m)_{i,j}$ indicates the pair-wise similarity between the anchor ($P_{w,i}^t$: weighted view of the i -th sample) and its positive/negative views ($P_{m,j}^t$: domain-specific views of the j -th sample). Here, the domain-specific view $P_{m,i}^t$ are named as *original positives* of the anchor as they originate from the same i -th sample. Notably, in addition to the dot product for similarity measurement, we adopt the softmax function with the temperature parameter $\text{tem} = 0.15$ to obtain the final values of each row. This allows views of other samples to compete with *original positives* to become “more positive” to the anchor. By minimizing the L1 distance between PLM and PCM, the Intra loss is formulated as:

$$\mathcal{L}_{Intra}(p^{sm}, p^t) = \text{Mean}(|\text{PL}_B^2 - \text{PC}_m|), \quad (9)$$

where $\text{Mean}(\cdot)$ computes the mean value across all elements in the matrix. The intrinsic mechanisms of \mathcal{L}_{Intra} are described as follows: (1) If samples i and j belong to different pseudo-classes, Eq. (9) for the i -th sample can be expressed as the term $\mathcal{L}_{intra(i,j)} = (1 - (\text{PC}_m)_{i,i}) + (\text{PC}_m)_{i,j}$. In this case, if $(\text{PC}_m)_{i,i} < (\text{PC}_m)_{i,j}$, it suggests that the original positive ($P_{m,i}^t$) lose in competition with the view of the j -th sample ($P_{m,j}^t$), implying an uncertain pseudo-label of i -th sample. Consequently, this term results in a larger loss value to correct this potentially erroneous pseudo-label, with the pseudo-class represented by the j -th sample potentially becoming the true class. Similarly, if $(\text{PC}_m)_{i,i} > (\text{PC}_m)_{i,j}$, this indicates that original positives maintain their dominant position, suggesting a relatively reliable pseudo-label for the i -th sample. (2) Conversely, if i and j belong to the same pseudo-class, Eq. (9) takes the form $\mathcal{L}_{intra(i,j)} = (1 - (\text{PC}_m)_{i,i}) + (1 - (\text{PC}_m)_{i,j})$. In this case, both $(\text{PC}_m)_{i,i}$ and $(\text{PC}_m)_{i,j}$ are optimized to have larger values to minimize this loss term.

TABLE I
COMPARISON OF CLASSIFICATION ACCURACY (%) ON OFFICE-31 AND OFFICE-HOME.

Datasets		Office-31				Office-Home				
Protocols	Methods	→D	→W	→A	Avg	→A	→C	→P	→R	Avg
Single Best	Source-only	99.3	96.7	62.5	86.2	65.3	49.6	79.7	75.4	67.5
	DAN [13]	99.5	96.8	66.7	87.7	68.2	56.5	80.3	75.9	70.2
	DANN [2]	99.1	96.9	68.2	88.1	67.0	53.6	80.3	76.3	69.3
Source Combine	DAN [13]	99.6	97.8	67.6	88.3	68.5	59.4	79.0	82.5	72.4
	DANN [2]	99.7	98.1	67.6	88.5	68.4	59.1	79.5	82.7	72.4
	D-CORAL [1]	99.3	98.0	67.1	88.1	68.1	58.6	79.5	82.7	72.2
Multi-Source	M ³ SDA [5]	99.3	98.0	67.2	88.2	66.2	58.6	79.5	81.4	71.4
	MFSAN [18]	99.5	95.5	72.7	90.2	72.1	62.0	80.3	81.8	74.1
	MIAN [4]	99.5	98.5	74.7	90.9	69.4	63.1	79.6	80.4	73.1
	T-SVDNet [44]	99.4	99.6	74.1	91.0	71.9	65.1	82.6	81.8	75.3
	SPS [45]	100.0	99.3	73.8	91.0	<u>75.1</u>	<u>66.0</u>	84.4	84.2	<u>77.4</u>
	DFSE [46]	99.4	98.8	73.2	90.5	73.4	62.7	<u>84.5</u>	<u>85.3</u>	76.5
	MIEM [50]	<u>99.8</u>	<u>99.7</u>	<u>75.9</u>	<u>91.7</u>	73.6	65.9	83.2	83.1	76.5
	A ³ MDA (ours)	100.0	99.8	77.9	92.6	75.4	66.3	85.6	85.4	78.2

In summary, when the PLM (PL_B^2) exhibits relatively smaller distances with PCM from different source-specific views (PC_m), the selected pseudo-labels for hard samples are more reliable. This process effectively rectifies the false pseudo-labels of those hard samples and largely avoids the excessive reliance on certain domain-specific predictions (views) in weighted predictions.

Training and Inference. During training, we employ cross-entropy loss \mathcal{L}_{cls} for all data predictions and their real/pseudo labels. By combining \mathcal{L}_{Inter} and \mathcal{L}_{Intra} using hyperparameters λ_1 and λ_2 for M source domains, the final objective function is:

$$\mathcal{L}_{total} = \sum_{m=1}^M (\lambda_1 \cdot \mathcal{L}_{Inter} + \lambda_2 \cdot \mathcal{L}_{Intra} + \mathcal{L}_{cls}), \quad (10)$$

For better understanding, we summarize the batch-wise training process in Algorithm 1. As for inference in the target domain, we directly utilize the weighted predictions as the final prediction results.

IV. EXPERIMENTS

To validate the generalizability and superiority of our A³MDA, we conduct comprehensive evaluations in this section using seven widely used publicly available datasets and compare the results with state-of-the-art methods.

A. Datasets

Office-31 [47] is a commonly used MDA dataset, with 4,110 images in 31 categories from three domains: Amazon (A), Webcam (W), and DSLR (D). This dataset is imbalanced, with 2,817, 795, and 498 images in domains A, W, and D, respectively. **Office-Home** [48] is a benchmark dataset for MDA tasks, containing 15,588 images across Artistic (A), Clip Art (C), Product (P), and Real-World (R) domains, covering 65 classes in total. **DomainNet** [5] is a challenging dataset with 345 categories and 6 domains, including Clipart (Clp), Infograph (Inf), Painting (Pnt), Quickdraw (Qdr), Real (Rel), and Sketch (Skt). **ImageCLEF-DA** [14] is a dataset with 12 categories shared by 3 public domains: Caltech-256 (C), ImageNet ILSVRC 2012 (I), and Pascal VOC 2012 (P). Each domain

TABLE II

COMPARISON OF CLASSIFICATION ACCURACY (%) ON DOMAINET.							
Methods	→Clp	→Inf	→Pnt	→Qdr	→Rel	→Skt	Avg
M ³ SDA [5]	58.6	26.0	52.3	6.3	62.7	49.5	42.6
T-SVDNet [44]	66.1	25.0	54.3	16.5	65.4	54.6	47.0
PTMDA [41]	66.0	28.5	58.4	13.0	63.0	54.1	47.2
SPS [45]	<u>70.8</u>	24.6	55.2	19.4	67.5	57.6	49.2
DSFE [46]	68.2	25.8	<u>58.8</u>	18.3	<u>71.9</u>	57.6	50.1
MIEM [50]	69.0	<u>28.6</u>	58.7	<u>20.5</u>	68.9	<u>59.2</u>	<u>50.8</u>
A ³ MDA(ours)	71.4	31.6	60.3	21.1	73.3	60.7	53.1

contains 600 images, and each category has 50 images. **PACS** [51] is a dataset that includes images from four domains: Art (A), Cartoon (C), Sketch (S), and Photo (P). Each domain contains 7 categories, with the following number of images: P (1,670 images), A (2,048 images), C (2,048 images), and S (3,929 images). **Digits-5** [5] dataset consists of handwritten digit images from five different domains: MNIST-M (mm), MNIST (mt), USPS (up), SVHN (sv), and SYN (syn). There are 10 classes in total, corresponding to the digits 0 to 9. **Office-Caltech** [52] dataset comprises four different domains: Webcam (W), DSLR (D), Caltech10 (C), and Amazon (A). The number of images in each domain is as follows: Webcam (157 images), DSLR (295 images), Caltech10 (1,123 images), and Amazon (958 images) with each domain containing 10 categories.

B. Implementation and Training Details

When implementing A³MDA, we employ diverse backbone networks (denoted as $F(\cdot)$) for different datasets to ensure consistency with other comparative methods. Specifically, for the Office-Caltech and DomainNet datasets, we utilize ResNet101 [53]. For the Digits-5 dataset, we adhere to the architecture proposed in M³SDA [5]. For the remaining datasets, we use ResNet50. All these backbone models are pretrained on ImageNet. For the domain-specific feature extractor $A_m(\cdot)$, we apply the (Conv1×1, Conv3×3, and Conv1×1) structure to reduce the number of channels from 2048 to 256. As for the classifier $C_m(\cdot)$, it comprises a single

TABLE III

COMPARISON OF CLASSIFICATION ACCURACY (%) ON IMAGECLEF-DA.

Protocols	Methods	→ P	→ C	→ I	Avg
Single Best	Source-only	74.8	91.5	83.9	83.4
	DAN [13]	75.0	93.3	86.2	84.8
	D-CORAL [1]	76.9	93.6	88.5	86.3
Source Combine	DAN [13]	77.6	93.3	92.2	87.7
	DANN [2]	77.9	93.7	91.8	87.8
Multi-Source	M ³ SDA [5]	77.3	94.3	91.9	88.0
	MFSAN [18]	79.1	95.4	93.6	89.4
	MIAN [4]	77.6	95.1	91.5	88.1
	T-SVDNet [44]	78.9	95.5	93.7	89.3
	PTMDA [41]	<u>79.1</u>	<u>97.3</u>	94.1	<u>90.2</u>
	DSFE [46]	78.7	96.0	93.5	89.4
	MIEM [50]	79.0	97.1	<u>94.3</u>	90.1
	A ³ MDA(ours)	79.7	97.8	97.5	91.7

TABLE IV

COMPARISON OF CLASSIFICATION ACCURACY (%) ON PACS.

Protocols	Methods	→ A	→ C	→ S	→ P	Avg
Source Combine	Source-only	85.16	76.78	71.22	97.94	82.77
	DAN [13]	87.35	83.92	77.07	98.32	86.67
	DANN [2]	87.53	84.21	78.44	97.64	86.96
Multi-Source	M ³ SDA [5]	84.20	85.68	74.62	94.47	84.74
	MFSAN [18]	90.19	90.47	81.53	97.23	89.85
	MIAN [4]	90.32	88.42	81.23	<u>98.71</u>	89.67
	T-SVDNet [44]	91.39	<u>91.39</u>	84.97	97.93	91.42
	DSFE [46]	90.43	90.71	85.59	98.60	91.33
	MIEM [50]	<u>91.87</u>	90.44	<u>88.07</u>	<u>98.71</u>	<u>92.27</u>
	A ³ MDA(ours)	92.14	91.56	90.35	99.30	93.34

fully connected layer that maps features with 256 channels from $A_m(\cdot)$ to the class space of the respective dataset.

When training A³MDA, we set the learning rate to 0.001 for the backbone $F(\cdot)$ pretrained on ImageNet, and 0.01 for the domain-specific modules $A_m(\cdot)$ and $C_m(\cdot)$ trained from scratch. Training lasts 200 epochs on an RTX 3090 GPU, following the optimizer and learning schedule in [18]. We maintain a fixed random seed of 10 over 3 runs and report the average results. We adjust λ_1 for \mathcal{L}_{Inter} asymptotically from 0 to 1 by the formula $\frac{2}{\exp(-\theta p)} - 1$ in [], where $\theta = 10$ and p is linearly changing from 0 to 1 as training iteration increases. Based on our trial study, we set λ_2 for \mathcal{L}_{Intra} as 0.7 and the pseudo-label threshold τ as 0.6. For the smoothing factor β in Smooth AHM, and the selection ratio R to filter harder samples, we set them to 0.8 and 0.4.

C. Comparative Experiments

In this section, we compare A³MDA with state-of-the-art single-source domain adaptation (SDA) and multi-source domain adaptation (MDA) algorithms. Specifically, two protocols are adopted to train SDA methods, including 1) Single Best, which reports the best result among all source domains, and 2) Source Combination, which naively combines all source domains and then performs single-source domain adaptation, while one protocol 3) Multi-Source for MDA

TABLE V

COMPARISON OF CLASSIFICATION ACCURACY (%) ON DIGITS-5.

Methods	→mm	→mt	→up	→sv	→syn	Avg
M ³ SDA [5]	72.8	98.4	96.1	81.3	89.6	87.7
MDDA [6]	78.6	98.8	93.9	79.3	79.3	88.1
LtC-MSDA [42]	85.6	99.0	98.3	83.2	93.0	91.8
STEM [29]	89.7	99.4	98.4	89.9	97.5	95.0
DIDA-Net [9]	85.7	99.3	98.6	91.7	97.3	94.5
A ³ MDA(ours)	92.2	99.3	98.7	91.4	96.2	95.6

TABLE VI

COMPARISON OF CLASSIFICATION ACCURACY (%) ON OFFICE-CALTECH.

Protocols	Methods	→ A	→ C	→ D	→ W	Avg
Source Combine	Source-only	86.1	87.8	98.3	99.0	92.8
	DAN [13]	94.8	89.7	98.2	99.3	95.5
	DANN [2]	94.8	89.7	98.2	99.3	95.5
Multi-Source	M ³ SDA [5]	94.5	92.2	99.2	98.9	96.4
	MFSAN [18]	95.4	93.8	<u>99.4</u>	<u>99.7</u>	97.1
	MIAN [4]	96.1	94.6	99.0	99.3	97.2
	T-SVDNet [44]	96.6	93.9	100.0	99.5	97.5
	STEM [29]	98.4	94.2	100.0	100.0	<u>98.2</u>
	DSFE [46]	95.4	94.6	<u>99.4</u>	99.5	97.2
	MIEM [50]	96.4	<u>96.0</u>	100.0	99.5	98.0
	A ³ MDA(ours)	<u>97.3</u>	97.7	100.0	100.0	98.7

methods. Source-Only refers to directly transferring the model trained in source domains to the target domain. Here, we select DAN [13], D-CORAL [1], DANN [2], for SDA methods, and M³SDA [5], MFSAN [18], MDDA [6], MIAN [4], T-SVDNet [44], PTMDA [41], SPS [45], DSFE [46], MIEM [50], LtC-MSDA [42], STEM [29], DIDA-Net [9] for MDA methods. To ensure fairness, we either directly quote the results of compared methods from their original papers or reproduce them using the released codes if the results on a specific dataset are not available. For all compared methods on each dataset, we maintain consistency by employing the same backbone architecture ($F(\cdot)$ in A³MDA) and data pre-processing routines. Notably, as some methods may excel on one dataset but not on others, we may introduce slight variations in the selection of compared methods for each dataset. To better highlight the superiority of our method, we use **bold** for the best results and underline for the second-best results when comparing classification accuracy across different datasets in Tables I to VI.

Classification Accuracy. We first compared the accuracy on each task across seven datasets. The results on **Office-31** and **Office-Home** are shown in Table I. For Office-31, our method attains the highest average accuracy of 92.6%, surpassing the second-best competitor MIEM by 0.9%. As for the Office-Home dataset, our proposed A³MDA also outperforms all comparative methods, surpassing the second-best method SPS by 0.8%.

The results on **DomainNet** are shown in Table II. Our method excels in all seven domains, claiming the top spot with a substantial lead of 2.3% over the second-best MIEM, achieving an impressive average accuracy of 53.1%.

TABLE VII

COMPARISON OF COMPUTATIONAL COMPLEXITY ON OFFICE-HOME.

Methods	Params (M)	MACs (G)	Training time (h)	Inference time (s)
M ³ SDA [5]	28.54	6.76	6.56	15.19
T-SVDNet [44]	28.82	6.69	6.60	15.24
DSFE [46]	28.04	6.60	6.41	15.56
A ³ MDA(ours)	28.30	6.96	7.08	15.38

The results on **ImageCLEF-DA** are shown in Table III. A³MDA excels across all domains, securing the top rank with an average accuracy of 91.7%. This outperforms the second-best method PTMDA by 1.5%. Notably, our method exhibits a substantial 3.2% lead over MIEM on the ‘→I’ task.

Table IV presents the results obtained on the **PACS** dataset. Our method outperforms the second-ranked method MIEM by a margin of 1.07%, achieving superior performance on three out of four tasks with an average accuracy of 93.34% across the four domains.

Table V showcases the results on the **Digits-5** dataset. Our method achieves the highest average accuracy of 95.6%, surpassing the second-best method, STEM, by 0.6%. Particularly, in the ‘→mm’ task, our method demonstrates a significant improvement of 2.5% compared to STEM.

The results on **Office-Caltech** are shown in Table VI. Our method achieves the best performance on three out of four tasks, obtaining an average accuracy of 98.7% across four domains and ranking first in the list.

Computational Complexity. We also conducted a thorough analysis of model size (e.g., Params), computational complexity (e.g., Multiply-Accumulate Operations, MACs), and time complexity (e.g., average running time in both the training and inference phases) on **Office-Home**. All methods are built upon the ResNet50 backbone and implemented on the Intel(R) i9-11900K and one RTX 3090 GPU.

As observed in Table VII, since A³MDA does not introduce additional modules with trainable parameters except for $A_m(\cdot)$ and $C_m(\cdot)$, it maintains comparable or even lower parameters compared with other methods. Regarding MACs, A³MDA involves adaptive hardness quantification through different hardness measurements and their utilization in various scenarios, resulting in a minimal increase of 0.28G MACs in computational demand compared with three compared methods. However, this growth is considered acceptable, given that the additional computations related to hardness values primarily pertain to batch-wise predictions rather than high-dimensional features. Besides, our method exhibits a significant average improvement of 3.8% over three methods on the Office-Home dataset (refer to Table I), showcasing superior performance with limited computational complexity escalation. Regarding time complexity, A³MDA presented slightly longer training times on the Office-Home dataset compared to other methods. However, due to the adoption of a simple backbone, our method achieved a comparable inference speed compared to other methods.

Overall, for all the aforementioned datasets, which cover almost all currently popular and widely used datasets for

TABLE VIII

ABLATION STUDY ON KEY COMPONENTS FOR AVERAGE ACCURACY (%) ON OFFICE-31 AND OFFICE-HOME.

Levels/ Scenarios	Methods	Office-31	Office-Home
	\mathcal{L}_{mmd} (Baseline)	88.1	73.3
Data	+ Aug w/o Adjusting	88.5	73.6
Augmentation	+ Aug w/ Adjusting	89.5	74.5
Inter-domain	+ \mathcal{L}_{mmd}^{WC} w/o Weighting	90.5	75.6
Alignment	+ \mathcal{L}_{mmd}^{WC} w/ Weighting	91.2	76.4
Intra-Domain	+ PCM w/o Selecting	91.9	77.6
Alignment	+ PCM w/ Selecting	92.6	78.2

multi-source domain adaptation classification tasks, A³MDA has consistently demonstrated state-of-the-art performance on average. Besides, experiment results on computation metrics also indicate that our method can achieve a better trade-off between performance and complexity. This serves as compelling evidence for the robustness and versatility of the proposed adaptive hardness strategy.

E. Ablation Studies

In this section, we conduct a thorough exploration of A³MDA from various perspectives. This exploration includes the examination of key components and their utilization, the assessment of different hardness measurements in various utilization scenarios, the exploration of hyperparameter settings, and various visualization experiments such as t-SNE, similarity matrix, and trends of hardness values during training.

Evaluation on Adaptive Hardness Utilization. To evaluate the effectiveness of various key components and their utilization in A³MDA, we conduct ablative experiments on the Office-31 and Office-Home datasets. We establish traditional MMD as our baseline (\mathcal{L}_{mmd}) and gradually incorporate three levels of components. ‘Aug’ denotes data augmentation, and ‘Adjusting’ involves using hardness values from Smooth AHM $\mathbf{S}(\cdot)$ for adaptive intensity adjustment. ‘ \mathcal{L}_{mmd}^{WC} ’ represents the weighted clustered MMD for inter-domain alignment, while ‘Weighting’ denotes the use of Comparative AHM $\mathbf{H}^c(\cdot)$ for sample-specific weights. PCM signifies the inclusion of a pseudo-contrastive matrix for intra-domain alignment, and ‘Selecting’ indicates whether Comparative AHM $\mathbf{H}(\cdot)$ is employed to choose more challenging samples for PCM formulation. As shown in Table VIII, relying solely on random strong data augmentation does not significantly improve the model due to the presence of over-augmentation. However, introducing the adjusting strategy enables dynamic adaptation of augmentation, leading to notable improvements of 1.4% and 2.2% over the baseline on Office-31 and Office-Home, respectively. For inter-domain alignment, we progressively incorporate sample-specific class attributes and hardness values to refine \mathcal{L}_{mmd} , leading to the formulation of \mathcal{L}_{mmd}^{WC} . This formulation significantly enhances the robustness and precision of the alignment process, contributing to a noteworthy improvement of 1.7% on Office-31 and 1.8% on Office-Home. For intra-domain alignment, integrating PCM improves the categorizability of the target domain feature space by fostering an internal competitive environment. Based

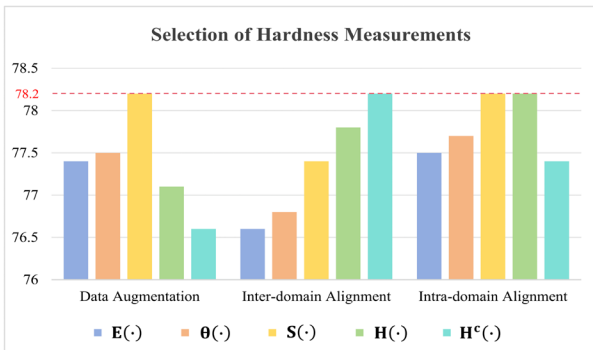


Fig. 5. Investigation of various AHMs on Office-Home.

on hardness rankings, further injecting a simple yet adaptive selection strategy externally intensifies the competition within PCM, aiding in the correction of erroneous pseudo-labels. This combined enhancement results in a significant 1.4% and 1.8% improvement on Office-31 and Office-Home.

Evaluation of Adaptive Hardness Quantification. A notable innovation in A^3 MDA involves the application of diverse Adaptive Hardness Measurements (AHMs) in various domain adaptation scenarios, resulting in remarkable results across multiple datasets. In A^3 MDA, we progressively introduce three different types of AHMs, including the Basic AHM $\theta(\cdot)$, the Smooth AHM $S(\cdot)$ utilizing a smoothing mechanism, and two Comparative AHMs ($H(\cdot)$ and $H^c(\cdot)$) employing single and dual-level comparison mechanisms. The optimal AHMs for three levels are $S(\cdot)$ in Data Augmentation, $H^c(\cdot)$ in inter-domain Alignment, and $H(\cdot)$ in intra-domain Alignment. Here, we explore the selection of AHMs at three levels using the Office-Home dataset. Specifically, for data augmentation, we construct dedicated memory banks for all AHMs to store values from the previous epoch, which are then utilized in Eq. (4). For inter-domain alignment, we assign different AHMs to source and target domain samples. In intra-domain alignment, we employ the sorting of different AHMs to construct a pseudo-contrastive matrix (PCM). Importantly, to obtain each result, we only modify the AHM used at the investigated level, ensuring that the other two AHMs continue to use their optimal configurations. Additionally, we introduce ordinary information entropy as $E(\cdot)$, serving as an additional basic AHM. The results of the exploration of various AHMs are depicted in Fig. 3.

For Data Augmentation, when compared to the optimal $S(\cdot)$, basic AHMs like $E(\cdot)$ (being normalized to $[0,1]$ to accommodate Eq. (4)) and $\theta(\cdot)$ without a smoothing mechanism lead to mediocre results. This is attributed to the instability caused by random fluctuations, as these AHMs solely provide assessments of sample hardness in the current epoch. Besides, further introducing comparative mechanisms in $H(\cdot)$ and $H^c(\cdot)$ over $S(\cdot)$ also fall short of achieving satisfactory outcomes when using them in augmentations. This is primarily because their effectiveness is heavily dependent on the difficulty of other samples within the batch from the previous epoch, and such relative difficulty values cannot serve as considerations for adaptive augmentations in the current epoch.

TABLE IX
COMPARISON OF DIFFERENT BACKBONES ON OFFICE-HOME.

Methods	$\rightarrow A$	$\rightarrow C$	$\rightarrow P$	$\rightarrow R$	Avg	Params	MACs
InceptionV3	77.1	66.7	85.3	85.6	78.7	29.87M	8.42G
DensNet161	79.3	67.5	85.7	86.1	79.7	31.42M	10.75G
ViT-B/16	79.0	67.9	86.1	86.8	80.0	90.31M	20.68G
ResNet34	74.2	65.0	83.2	83.1	76.4	24.14M	5.70G
ResNet101	77.8	67.8	85.5	85.5	79.2	47.29M	10.69G
A^3 MDA (ours)	75.4	66.3	85.6	85.4	78.2	28.30M	6.96G

TABLE X
ABLATION STUDY OF DIFFERENT METRIC DISTANCES FOR AVERAGE ACCURACY (%) ON OFFICE-HOME.

Methods	$\rightarrow A$	$\rightarrow C$	$\rightarrow P$	$\rightarrow R$	Avg
L2 [68]	58.7	45.8	67.6	68.8	60.2
L2 + Ours	62.8	53.7	73.4	74.4	66.1 ($\uparrow 5.9$)
WAS [69]	71.1	62.0	81.1	80.3	73.6
WAS + Ours	75.5	64.4	84.9	85.5	77.6 ($\uparrow 4.0$)
CORAL [1]	71.4	61.9	79.7	80.7	73.4
CORAL + Ours	75.0	64.5	85.5	85.3	78.0 ($\uparrow 4.6$)
MMD [18]	71.1	61.9	79.3	80.8	73.3
MMD + Ours	75.4	66.3	85.6	85.4	78.2 ($\uparrow 4.9$)

For Inter-domain Alignment, we found that AHMs with comparative mechanisms can automatically balance the batch-wise importance among different samples in the weighted MMD loss, thus enhancing batch-based optimization. Meanwhile, $H^c(\cdot)$, which builds upon $H(\cdot)$ but further introduces cluster-wise comparison, achieves better results by adaptively fostering intra-class convergence while promoting inter-class divergence.

For Intra-domain alignment, we found that Basic AHMs like $E(\cdot)$ and $\theta(\cdot)$ do not perform well due to their inability to stably and reliably perceive the hardness of target samples. Consequently, constructing an effective PCM became challenging. Interestingly, employing $H(\cdot)$ and maintaining $S(\cdot)$ both yield optimal performance, as the hardness ranking of samples within batches remained unchanged after batch-wise comparison. However, the further introduction of cluster-wise comparison in $H^c(\cdot)$ results in the poorest performance. This is because utilizing $H^c(\cdot)$ to select harder samples may lead to an unstable prioritization of batch-wise clusters with a limited number of target samples, thereby rendering the selection process almost ineffective.

Exploring Different Backbone Architectures. We experimented with various backbone architectures on the Office-Home dataset, including InceptionV3 [65], DenseNet161 [66], ViT-B/16 [67], ResNet34 [53], and ResNet101 [53], which vary in complexity and design philosophies. The original A^3 MDA utilized ResNet50 [53], consistent with prior MDA studies [18, 45, 46]. As detailed in TABLE IX, our method can adapt well to different backbones and achieve competitive performance across all of them. These findings underscore the wide applicability of our method across various extraction backbones.

Exploring Different Discrepancy Metrics. The choice of discrepancy metrics is pivotal in discrepancy-based MDA

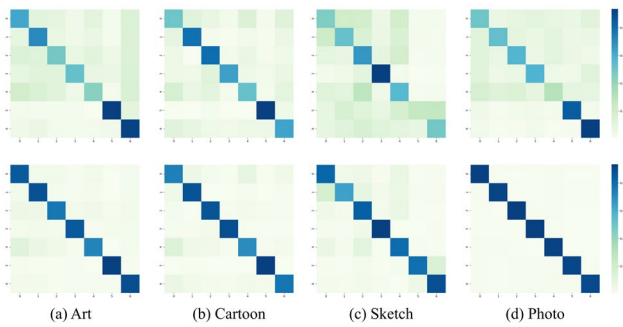


Fig. 6. Visualizations of similarity matrices on PACS.

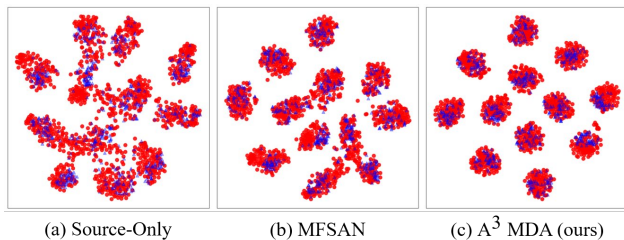


Fig. 7. The t-SNE visualizations of feature embeddings on ‘→I’ task on ImageCLEF-DA (red: source; blue: target).

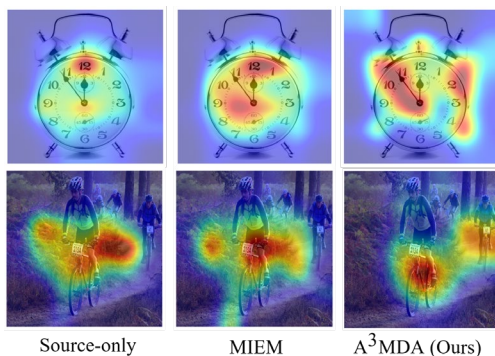


Fig. 8. Visualization of Grad-CAM on real-world images.

methods. In A^3MDA , we compared traditional metrics—L2 distance [68] (‘L2’), Wasserstein distance [69] (‘WAS’), and CORAL [1] (Correlation Alignment)—with MMD on the Office-Home dataset. Results in Table X consistently demonstrate performance enhancements across these methods when employing our hardness-driven strategies, resulting in improvements of 5.9%, 4.0%, 4.6%, and 4.9%. These results affirm the potential of our approach in enhancing various conventional discrepancy-based MDA methods.

Visualization of Similarity Matrix. We present prototypical similarity matrices for four domains from the PACS dataset. As observed in Fig. 6, A^3MDA outperforms the Source-only baseline (top row) in capturing the underlying cluster-wise relationships, resulting in prominently reduced domain-specific noise in the matrices (bottom row). Notably, the noise reduction is most pronounced in the Photo domain, attributed to our cluster-level constraint that precisely performs intra domain alignment in the pseudo-contrastive matrix, thereby enhancing its discriminative capability.

Visualization of Feature Embeddings. To validate the transferability of our model, we utilize t-SNE visualizations to depict the feature embeddings of different methods on the ‘→I’

task of the ImageCLEF-DA dataset. As shown in Fig. 7, the target features learned by the Source-Only model exhibit a mismatch with the source domain. In contrast, our proposed method outperforms both Source-Only and MFSAN methods, evidenced by its generation of clusters with sharper boundaries. This demonstrates its superior transferability on the target domain while maintaining strong discrimination ability and performance.

Visualization of Class Activation Mapping. To enhance the interpretability, we present Grad-CAM results for two real-world images, depicted in Fig. 8. For alarm clocks (top row), our method sharply focuses on clock hands and partial circular edges, capturing crucial discriminative features. For bicycles (bottom row), our approach identifies and highlights both the front and back bicycles accurately, a detail overlooked by other methods. Overall, our approach effectively emphasizes features crucial for accurate classification.

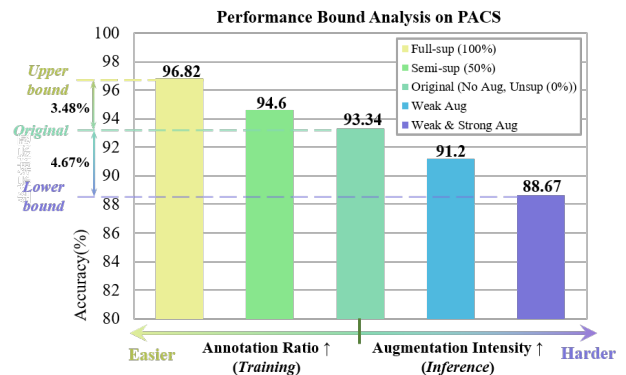


Fig. 9. Bound Analysis of performance on PACS.

Performance Bound Analysis. We conducted a bound analysis on PACS, which builds upper and lower bounds through varied approaches. For the upper bound, considering our model tackles an unsupervised setting where ground truth labels of the target domain are unseen during training, we progressively increased the proportion of visible labels to approximate peak performance. Specifically, we examined three annotation ratios: 0% (original unsupervised scenario), 50% (semi-supervised scenario, ‘Semi-sup’), and 100% (fully supervised scenario, ‘Full-sup’, representing the upper bound). As for the lower bound, we applied diverse forms of data augmentation (aligned with those detailed in the methodology) to target domain samples during the inference stage to simulate extreme scenarios. Specifically, we considered three forms: no augmentation (original), weak augmentation (‘Weak Aug’), and weak plus strong augmentation (‘Weak & Strong Aug’, representing the lower bound). As shown in Fig. 9, our method closely approaches the upper bound in the original unsupervised setting, with only a small gap of 3.48%. Besides, under strong noise perturbations, the performance only decreased by an average of 4.67%. This resilience can be attributed to our adaptive augmentation strategy, which effectively handles hard samples and ensures accurate predictions even under substantial perturbations. The above analysis underscores A^3MDA ’s robust adaptability across varying levels of data availability and noise.

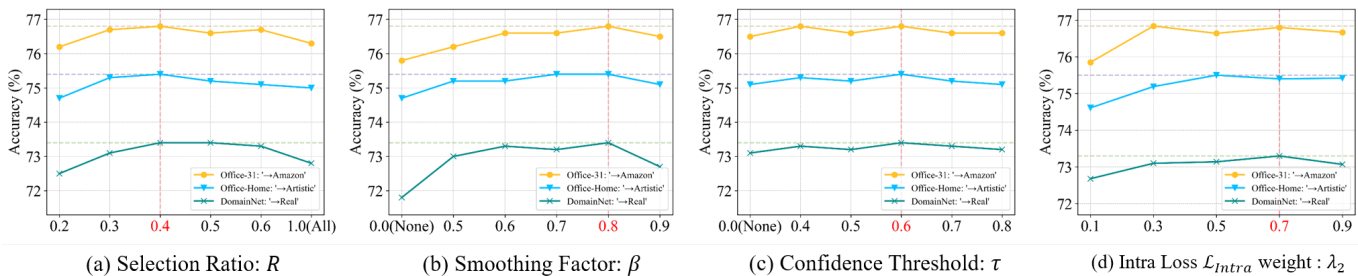


Fig. 11. Analysis of a) selection ratio R , b) smoothing factor β , c) pseudo-label threshold τ and d) Intra loss weight λ_2 on three tasks (‘→Amazon’ of Office-31; ‘→Artistic’ of Office-Home; ‘→Real’ of DomainNet).

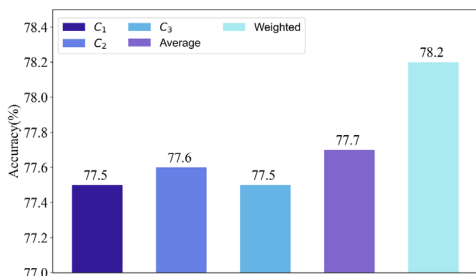


Fig. 10. Analysis of weighted prediction on Office-Home.

Analysis of Prediction Approaches. We also explore different prediction approaches used for inference. Apart from the weighted prediction $P_{w,i}^t$ used in A³MDA (referred to as ‘Weighted’), we also consider the predictions $P_{m,i}^t$ generated by each domain-specific classifier $C_m(\cdot)$, as well as the average combination of these predictions $P_{a,i}^t = \frac{1}{M} \sum_{m=1}^M P_{m,i}^t$ (referred to as ‘Average’). As depicted in Fig. 10, the weighted prediction performs the best as it dynamically determines the reliance of the target domain on different source domains based on their respective qualities. In contrast, solely relying on predictions from a domain-specific classifier $C_m(\cdot)$ or treating each domain equally without tailored processing with ‘Average’, would result in a biased or impartial approach that cannot achieve the benefits provided by dynamic weights w_m , leading to sub-optimal performance.

Hyperparameters tuning strategies. Our method employs a comprehensive three-level framework, necessitating the determination of multiple hyperparameters. Traditionally, a grid search approach across these hyperparameters could potentially enhance performance but is notably time-consuming and labor-intensive. Therefore, we adopted diverse tuning strategies to streamline the selection process:

(1) Formula-based tuning for \mathcal{L}_{Inter} : For λ_1 , which governs the inter-domain alignment loss term \mathcal{L}_{Inter} , we applied a formula-based tuning strategy similar to DANN [2], using the adaptive formula $\lambda_1 = \frac{2}{\exp(-\theta p)} - 1$ instead of a fixed value. According to [2], this tuning formula, along with the setting of $\theta = 10$, can effectively stabilize sensitivity during the early stages and has demonstrated success across several prominent MDA approaches (e.g., MFSAN [18]) for managing inter-domain alignment constraints.

(2) Equalize weights of two MMD terms: Initially, we introduced an additional hyperparameter η to independently control the weighted clustered term in Eq. (7), transforming it

to the form $\mathcal{L}_{Inter} = \mathcal{L}_{mmd} + \eta \cdot \mathcal{L}_{mmd}^{WC}$. Experimental findings indicated optimal model performance is observed when maintaining a balanced ratio of η (within the range of [0.8 – 1.2]), with deviations outside this range resulting in slight performance decreases. Therefore, to simplify parameter tuning, we set η to 1.0 (which can be seen as an omission).

(3) Individual tuning with appropriate tasks: For the remaining hyperparameters, we individually tune them across multiple appropriate tasks (domains). We adhere to the following criteria to select domains: (1) The selected domains are of moderate scale, facilitating effective tuning; (2) The selected domains pose significant challenges (e.g., the ‘Amazon’ task in Office-31 is particularly challenging); (3) The characteristics of the selected domains are similar to those found in other datasets (e.g., the ‘Real’ domain in DomainNet is also present in Office-Home). Ultimately, we selected three tasks (‘Amazon’ from Office-31, ‘Artistic’ from Office-Home, and ‘Real’ from DomainNet).

As observed from Fig. 11(a), adjusting R to incorporate a fraction of more challenging samples enhances internal competition within PCM, facilitating the correction of erroneous pseudo-labels. Nevertheless, excessively small ratios ($R \leq 0.3$) also lead to a decline in performance, as the limited number of samples hinders effective competition.

According to Fig. 11(b), setting β to 0 (i.e., replacing Smooth AHM with Basic AHM) may induce over-augmentation and performance decline due to the instability of instantaneous hardness measurements. Moreover, the commonly used value of 0.9 in standard EMA is not optimal, as an excessively large β may overly smoothen hardness variations, complicating the adaptation of the model.

For τ , unlike other pseudo-labeling approaches that are susceptible to varying threshold configurations, our method maintains a consistent accuracy within a narrow deviation of 0.5% across three datasets, as shown in Fig. 11(c). This stability is attributed to A³MDA’s ability to gradually improve the quality of pseudo-labels through the proposed PCM.

For λ_2 , which controls \mathcal{L}_{Intra} , we selected candidate values for λ_2 from the set {0.1, 0.3, 0.5, 0.7, 0.9} and explore it on three specific tasks. As observed in Fig. 11(d), the overall best results consistently emerge around 0.7.

In conclusion, optimal performance is achieved with $R = 0.4$, $\beta = 0.8$, $\tau = 0.6$, $\lambda_2 = 0.7$. Notably, these hyperparameters remained consistent across all seven datasets, delivering state-of-the-art performance in each. This indicates

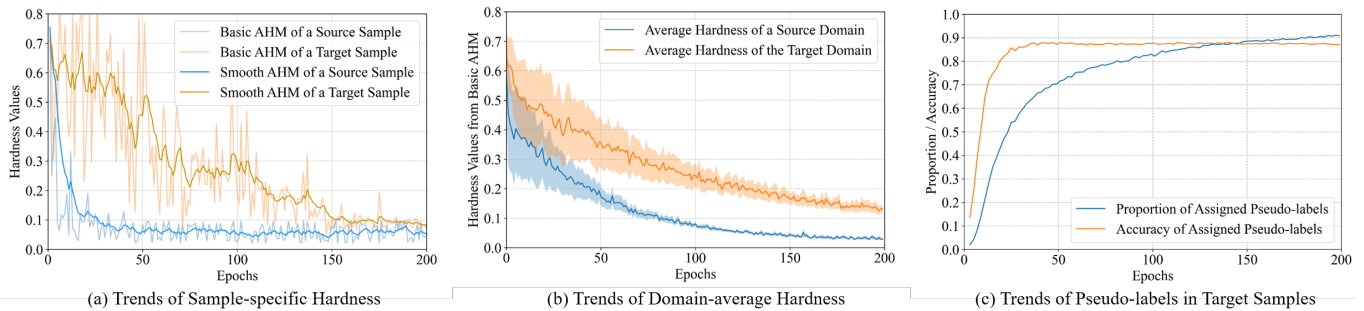


Fig. 12. Trends of hardness values and pseudo-labels. (a) displays hardness values for a pair of samples from the target domain (Real) and one source domain (Clipart) in the ‘ \rightarrow Real’ task of DomainNet. (b) illustrates average hardness in the above two domains. (c) presents the trends in accuracy and assignment rate of pseudo-labels of the target domain (Product) in ‘ \rightarrow Product’ task of Office-Home.

the strong generalizability of our chosen hyperparameter and the effectiveness of our optimization strategies, minimizing the necessity for task-specific adjustments.

Analysis on Hardness Values. We display the trends of perceived sample-specific and domain-average hardness in Fig. 12(a) and Fig. 12(b). As observed, the Basic AHM of sample-specific hardness shows pronounced fluctuations or rebounds during early training. This inadequacy results in the model’s initial inability to handle certain strong perturbations randomly selected from an augmentation pool in our adaptive strategy, leading to unstable predictions with low confidence. However, as training progresses, the model becomes well-fitted to both source and target samples, generating more confident predictions even under complex augmentation. Consequently, Basic AHM values exhibit decreasing trends and reduced fluctuations over time. In contrast, values from Smooth AHM are considerably smoother than those from Basic AHM, providing a more stable measurement of sample-specific hardness. As for domain-average hardness, both the mean and standard deviation of Basic AHM values decrease for both domains as training progresses. This reduction in perceived hardness values also correlates with increased data augmentation intensity, which demonstrates the enhanced generalization ability of our model.

Analysis on trends in pseudo-labels. Fig. 12(c) depicts the trends of pseudo-labels in target samples. It is observed that during the initial training phase of A³MDA, both the proportion of assigned pseudo-labels and their accuracy increase rapidly. In the later stages of training, while the proportion of assigned pseudo-labels continues to rise, our model maintains stable pseudo-label accuracy as it handles an increasing number of labeled target samples. This can be attributed to the effectiveness of our alignment strategies in addressing erroneous pseudo-labels.

V. DISCUSSION

In this paper, we introduce A³MDA, a novel framework for the MDA classification task. A³MDA systematically addresses three commonly overlooked aspects: 1) the potential of data augmentation, 2) the importance of intra-domain alignment, and 3) the design of cluster-level constraints. To tackle these issues, we propose a series of Adaptive Hardness-driven Strategies. For hardness quantification, we develop three progressive Adaptive Hardness Measurements, i.e. Basic,

Smooth, and Comparative AHMs. Unlike traditional methods that solely rely on entropy as the hardness metric, our AHMs introduce new features at each stage of progression. As for hardness utilization, instead of using measured hardness values merely for conventional filtering, we adaptively incorporate hardness values to address the aforementioned aspects in both Augmentation and Alignment scenarios through three types of Actions. Specifically, considering that traditional augmentation methods do not adapt to the dynamic hardness of samples and the evolving generalization capability of the model, our Smooth AHM adjusts the intensity of adaptive strong augmentation to prevent over-augmentation. Furthermore, to improve upon current loss designs that overlook sample-specific attributes, we utilize hardness values from Comparative AHM along with class attributes to facilitate cluster-level constraints.

A³MDA demonstrates broad practical applicability across three aspects. Firstly, in terms of dataset selection, we chose seven datasets that cover a wide range of real-world domains with diverse data distributions. Our A³MDA demonstrates state-of-the-art performance across all these benchmarks, showcasing its robustness in diverse real-world application environments. Secondly, our model effectively mitigates noise interference by adaptively incorporating various types of strong augmentation or noise (e.g. Gaussian noise, salt-pepper noise, blurring) during training. This is reflected in the experimental results. Thirdly, we also experimented with applying our hardness-driven framework to other feature extraction architectures or alignment constraints (i.e. divergence loss). We found that these substitutions also yield excellent performance and lead to significant improvements compared to their respective baseline. These findings underscore the broad applicability of our proposed hardness strategies in MDA classification tasks.

Despite its excellent performance, A³MDA still faces several limitations. Firstly, the proposed hardness-driven strategies necessitate the matching of the most suitable quantification metric (AHM) for each utilization scenario, which may involve cumbersome manual experimentation. Therefore, A³MDA thoroughly considers the characteristics introduced at each stage of AHM progression, along with the required functionalities for actions in augmentation and alignment scenarios, thus streamlining this matching process. Furthermore, due to the comprehensive nature of the proposed

framework, A³MDA inherently deals with multiple operations and constraints, complicating the hyperparameter selection process. To address this, we utilized several tuning strategies to expedite the selection process, ultimately achieving a relatively optimal configuration across all datasets within a shorter timeframe. We also anticipate future research into more efficient and optimal methods for tuning hyperparameters within the hardness-driven framework. Finally, our MDA analysis framework exclusively targets natural image classification and does not include tasks such as image segmentation or other fields like medical applications. With this in mind, we aspire for our work to set a paradigm for future MDA research, where researchers can refer to its hardness-driven strategies and adapt or enhance its elements for broader fields and applications.

V. CONCLUSION

In this paper, we present a novel hardness-driven strategy for Multi-source Domain Adaptation, named A³MDA, to address three key aspects of conventional MDA methods. A³MDA centers around adaptive quantification and utilization of hardness values. For quantification, we introduce three progressive Adaptive Hardness Measurements (AHM), i.e., Basic, Smooth, and Comparative AHMs, to provide effective assessments of the hardness of individual source/target samples. For utilization, we incorporate and adapt hardness values to various augmentation and alignment scenarios. This involves adjusting the intensity level of data augmentation, using hardness values as weights to create a weighted-clustered Maximum Mean Discrepancy loss for inter-domain alignment, and selecting harder samples to form a pseudo-contrastive matrix for intra-domain alignment. Experiments on multiple datasets showcase the potential of our adaptive hardness-driven strategy.

REFERENCES

- [1] B. Sun and K. Saenko, "Deep coral: Correlation alignment for deep domain adaptation," in *Computer Vision—ECCV 2016 Workshops: Amsterdam, The Netherlands, October 8–10 and 15–16, 2016, Proceedings, Part III 14*. Springer, 2016, pp. 443–450.
- [2] Y. Ganin and L. Victor, "Unsupervised domain adaptation by backpropagation," *International conference on machine learning*. PMLR, 2015.
- [3] Y. Zhu, F. Zhuang, J. Wang, G. Ke, J. Chen, J. Bian, H. Xiong, and Q. He, "Deep subdomain adaptation network for image classification," *IEEE transactions on neural networks and learning systems*, vol. 32, no. 4, pp. 1713–1722, 2020.
- [4] G. Y. Park and S. W. Lee, "Information-theoretic regularization for multi-source domain adaptation," in *Proceedings of the IEEE/CVF International Conference on Computer Vision*, 2021, pp. 9214–9223.
- [5] X. Peng, Q. Bai, X. Xia, Z. Huang, K. Saenko, and B. Wang, "Moment matching for multi-source domain adaptation," in *Proceedings of the IEEE/CVF international conference on computer vision*, 2019, pp. 1406–1415.
- [6] S. Zhao, G. Wang, S. Zhang, Y. Gu, Y. Li, Z. Song, P. Xu, R. Hu, H. Chai, and K. Keutzer, "Multi-source distilling domain adaptation," in *Proceedings of the AAAI Conference on Artificial Intelligence*, vol. 34, no. 07, 2020, pp. 12 975–12 983.
- [7] S. Chen, "Multi-source domain adaptation with mixture of joint distributions," *Pattern Recognition*, p. 110295, 2024.
- [8] B. Gong, K. Grauman, and F. Sha, "Connecting the dots with landmarks: Discriminatively learning domain-invariant features for unsupervised domain adaptation," in *International conference on machine learning*. PMLR, 2013, pp. 222–230.
- [9] Z. Deng, K. Zhou, D. Li, J. He, Y.-Z. Song, and T. Xiang, "Dynamic instance domain adaptation," *IEEE Transactions on Image Processing*, vol. 31, pp. 4585–4597, 2022.
- [10] L. Zhou, M. Ye, D. Zhang, C. Zhu, and L. Ji, "Prototype-based multisource domain adaptation," *IEEE Transactions on Neural Networks and Learning Systems*, vol. 33, no. 10, pp. 5308–5320, 2021.
- [11] R. Xu, Z. Chen, W. Zuo, J. Yan, and L. Lin, "Deep cocktail network: Multi-source unsupervised domain adaptation with category shift," in *Proceedings of the IEEE conference on computer vision and pattern recognition*, 2018, pp. 3964–3973.
- [12] B. Sun, J. Feng, and K. Saenko, "Correlation alignment for unsupervised domain adaptation," *Domain adaptation in computer vision applications*, pp. 153–171, 2017.
- [13] M. Long, Y. Cao, J. Wang, and M. Jordan, "Learning transferable features with deep adaptation networks," in *International conference on machine learning*. PMLR, 2015, pp. 97–105.
- [14] M. Long, H. Zhu, J. Wang, and M. I. Jordan, "Deep transfer learning with joint adaptation networks," in *International conference on machine learning*. PMLR, 2017, pp. 2208–2217.
- [15] Y. Xu, M. Kan, S. Shan, and X. Chen, "Mutual learning of joint and separate domain alignments for multi-source domain adaptation," in *Proceedings of the IEEE/CVF Winter Conference on Applications of Computer Vision*, 2022, pp. 1890–1899.
- [16] J. Yuan, Y. Liu, C. Shen, Z. Wang, and H. Li, "A simple baseline for semi-supervised semantic segmentation with strong data augmentation," in *Proceedings of the IEEE/CVF International Conference on Computer Vision*, 2021, pp. 8229–8238.
- [17] Y. Zhu, F. Zhuang, J. Wang, J. Chen, Z. Shi, W. Wu, and Q. He, "Multi-representation adaptation network for cross-domain image classification," *Neural Networks*, vol. 119, pp. 214–221, 2019.
- [18] Y. Zhu, F. Zhuang, and D. Wang, "Aligning domain-specific distribution and classifier for cross-domain classification from multiple sources," in *Proceedings of the AAAI conference on artificial intelligence*, vol. 33, no. 01, 2019, pp. 5989–5996.
- [19] H. Yan, Y. Ding, P. Li, Q. Wang, Y. Xu, and W. Zuo, "Mind the class weight bias: Weighted maximum mean discrepancy for unsupervised domain adaptation," in *Proceedings of the IEEE conference on computer vision and pattern recognition*, 2017, pp. 2272–2281.
- [20] T.-H. Vu, H. Jain, M. Bucher, M. Cord, and P. Pérez, "Advent: Adversarial entropy minimization for domain adaptation in semantic segmentation," in *Proceedings of the IEEE/CVF conference on computer vision and pattern recognition*, 2019, pp. 2517–2526.
- [21] A. Ma, J. Li, K. Lu, L. Zhu, and H. T. Shen, "Adversarial entropy optimization for unsupervised domain adaptation," *IEEE Transactions on Neural Networks and Learning Systems*, vol. 33, no. 11, pp. 6263–6274, 2021.
- [22] J.-C. Su, Y.-H. Tsai, K. Sohn, et al., "Active adversarial domain adaptation," in *Proceedings of the IEEE/CVF Winter Conference on Applications of Computer Vision*, 2020, pp. 739–748.
- [23] S. Teng, Z. Zheng, N. Wu, L. Fei, and W. Zhang, "Domain adaptation via incremental confidence samples into classification," *International Journal of Intelligent Systems*, vol. 37, no. 1, pp. 365–385, 2022.
- [24] K. Huang, J. Geng, W. Jiang, X. Deng, and Z. Xu, "Pseudo-loss confidence metric for semi-supervised few-shot learning," in *Proceedings of the IEEE/CVF International Conference on Computer Vision*, 2021, pp. 8671–8680.
- [25] E. Tzeng, J. Hoffman, K. Saenko, et al., "Adversarial discriminative domain adaptation," in *Proceedings of the IEEE conference on computer vision and pattern recognition*, 2017, pp. 7167–7176.
- [26] M.-Y. Liu and O. Tuzel, "Coupled generative adversarial networks," *Advances in neural information processing systems*, vol. 29, 2016.
- [27] K. Saito, K. Watanabe, Y. Ushiku, and T. Harada, "Maximum classifier discrepancy for unsupervised domain adaptation," in *Proceedings of the IEEE conference on computer vision and pattern recognition*, 2018, pp. 3723–3732.
- [28] K. Li, J. Lu, H. Zuo, and G. Zhang, "Multi-source contribution learning for domain adaptation," *IEEE Transactions on Neural Networks and Learning Systems*, vol. 33, no. 10, pp. 5293–5307, 2021.
- [29] V.-A. Nguyen, T. Nguyen, T. Le, Q. H. Tran, and D. Phung, "Stem: An approach to multi-source domain adaptation with guarantees," in *Proceedings of the IEEE/CVF International Conference on Computer Vision*, 2021, pp. 9352–9363.

- [30] Y. Yuan, K. Yang, and C. Zhang, "Hard-aware deeply cascaded embedding," in *Proceedings of the IEEE international conference on computer vision*, 2017, pp. 814–823.
- [31] C. Sakaridis, D. Dai, S. Hecker, and L. Van Gool, "Model adaptation with synthetic and real data for semantic dense foggy scene understanding," in *Proceedings of the european conference on computer vision (ECCV)*, 2018, pp. 687–704.
- [32] F. Pan, I. Shin, F. Rameau, S. Lee, and I. S. Kweon, "Unsupervised intra-domain adaptation for semantic segmentation through self-supervision," in *Proceedings of the IEEE/CVF Conference on Computer Vision and Pattern Recognition*, 2020, pp. 3764–3773.
- [33] Y. Wang, C. Xu, C. Liu, et al., "Instance credibility inference for few-shot learning," in *Proceedings of the IEEE/CVF conference on computer vision and pattern recognition*, 2020, pp. 12 836–12 845.
- [34] Z. Zhao, S. Long, J. Pi, J. Wang, and L. Zhou, "Instance-specific and model-adaptive supervision for semi-supervised semantic segmentation," in *Proceedings of the IEEE/CVF Conference on Computer Vision and Pattern Recognition*, 2023, pp. 23 705–23 714.
- [35] B. Xie, L. Yuan, S. Li, C. H. Liu, and X. Cheng, "Towards fewer annotations: Active learning via region impurity and prediction uncertainty for domain adaptive semantic segmentation," in *Proceedings of the IEEE/CVF Conference on Computer Vision and Pattern Recognition*, 2022, pp. 8068–8078.
- [36] K. Zhou, Y. Yang, Y. Qiao, and T. Xiang, "Mixstyle neural networks for domain generalization and adaptation," *International Journal of Computer Vision*, pp. 1–15, 2023.
- [37] H. Zhang, M. Cisse, Y. N. Dauphin, and D. Lopez-Paz, "mixup: Beyond empirical risk minimization," in *International Conference on Learning Representations*, 2018. [Online]. Available: <https://openreview.net/forum?id=r1Ddp1-Rb>
- [38] S. Yun, D. Han, S. J. Oh, S. Chun, J. Choe, and Y. Yoo, "Cutmix: Regularization strategy to train strong classifiers with localizable features," in *Proceedings of the IEEE/CVF international conference on computer vision*, 2019, pp. 6023–6032.
- [39] E. D. Cubuk, B. Zoph, D. Mane, V. Vasudevan, and Q. V. Le, "Autoaugment: Learning augmentation strategies from data," in *Proceedings of the IEEE/CVF conference on computer vision and pattern recognition*, 2019, pp. 113–123.
- [40] E. D. Cubuk, B. Zoph, J. Shlens, and Q. V. Le, "Randaugment: Practical automated data augmentation with a reduced search space," in *Proceedings of the IEEE/CVF conference on computer vision and pattern recognition workshops*, 2020, pp. 702–703.
- [41] C.-X. Ren, Y.-H. Liu, X.-W. Zhang, and K.-K. Huang, "Multi-source unsupervised domain adaptation via pseudo target domain," *IEEE Transactions on Image Processing*, vol. 31, pp. 2122–2135, 2022.
- [42] H. Wang, M. Xu, B. Ni, et al., "Learning to combine: Knowledge aggregation for multi-source domain adaptation," in *Computer Vision—ECCV 2020: 16th European Conference, Glasgow, UK, August 23–28, 2020, Proceedings, Part VIII 16*. Springer, 2020, pp. 727–744.
- [43] Z.-G. Liu, L.-B. Ning, and Z.-W. Zhang, "A new progressive multisource domain adaptation network with weighted decision fusion," *IEEE Transactions on Neural Networks and Learning Systems*, 2022.
- [44] R. Li, X. Jia, J. He, S. Chen, and Q. Hu, "T-svdnet: Exploring high-order prototypical correlations for multi-source domain adaptation," in *Proceedings of the IEEE/CVF International Conference on Computer Vision*, 2021, pp. 9991–10 000.
- [45] Z. Wang, C. Zhou, B. Du, and F. He, "Self-paced supervision for multi-source domain adaptation," in *Proceedings of the Thirty-First International Joint Conference on Artificial Intelligence, IJCAI-22*, 2022.
- [46] K. Wu, F. Jia, and Y. Han, "Domain-specific feature elimination: multi-source domain adaptation for image classification," *Frontiers of Computer Science*, vol. 17, no. 4, p. 174705, 2023.
- [47] K. Saenko, B. Kulis, M. Fritz, et al., "Adapting visual category models to new domains," in *Computer Vision—ECCV 2010: 11th European Conference on Computer Vision, Heraklion, Crete, Greece, September 5–11, 2010, Proceedings, Part IV 11*. Springer, 2010, pp. 213–226.
- [48] H. Venkateswara, J. Eusebio, S. Chakraborty, and S. Panchanathan, "Deep hashing network for unsupervised domain adaptation," in *Proceedings of the IEEE conference on computer vision and pattern recognition*, 2017, pp. 5018–5027.
- [49] Z. Liu, S. Li, D. Wu, Z. Liu, Z. Chen, L. Wu, and S. Z. Li, "Automix: Unveiling the power of mixup for stronger classifiers," in *ECCV 2022*. Springer, 2022, pp. 441–458.
- [50] L. Wen, S. Chen, M. Xie, C. Liu, and L. Zheng, "Training multi-source domain adaptation network by mutual information estimation and minimization," *Neural Networks*, vol. 171, pp. 353–361, 2024.
- [51] D. Li, Y. Yang, Y.-Z. Song, and T. M. Hospedales, "Deeper, broader and artier domain generalization," in *Proceedings of the IEEE international conference on computer vision*, 2017, pp. 5542–5550.
- [52] B. Gong, Y. Shi, F. Sha, and K. Grauman, "Geodesic flow kernel for unsupervised domain adaptation," in *2012 IEEE conference on computer vision and pattern recognition*. IEEE, 2012, pp. 2066–2073.
- [53] K. He, X. Zhang, S. Ren, and J. Sun, "Deep residual learning for image recognition," in *Proceedings of the IEEE conference on computer vision and pattern recognition*, 2016, pp. 770–778.
- [54] Lu Y, Zhu Q, Zhang B, et al., "Weighted correlation embedding learning for domain adaptation," *IEEE Transactions on Image Processing*, vol.31, pp. 5303-5316, 2022.
- [55] Lu Y, Wong W K, Yuan C, et al., "Low-Rank Correlation Learning for Unsupervised Domain Adaptation," *IEEE Transactions on Multimedia*, 2023.
- [56] Lu Y, Wong W K, Zeng B, et al., "Guided discrimination and correlation subspace learning for domain adaptation," *IEEE Transactions on Image Processing*, vol.32, pp. 2017-2032, 2023.
- [57] Nguyen V, Le T, Tantithamthavorn C, et al., "Deep Domain Adaptation With Max-Margin Principle for Cross-Project Imbalanced Software Vulnerability Detection," *ACM Transactions on Software Engineering and Methodology*, 2024.
- [58] Nguyen T, Nguyen V, Le T, et al., "A Class-aware Optimal Transport Approach with Higher-Order Moment Matching for Unsupervised Domain Adaptation," *arXiv preprint arXiv:2401.15952*, 2024.
- [59] Yang M, Li Y, Zhang C, et al., "Test-time Adaptation against Multimodal Reliability Bias," *The Twelfth International Conference on Learning Representations*. 2024.
- [60] Li J, Li G, Shi Y, et al., "Cross-domain adaptive clustering for semi-supervised domain adaptation," *Proceedings of the IEEE/CVF Conference on Computer Vision and Pattern Recognition*, 2021, pp. 2505-2514.
- [61] Sun Z, Zhang H, Bai J, et al., "A discriminatively deep fusion approach with improved conditional GAN (im-cGAN) for facial expression recognition," *Pattern Recognition*, 135, pp. 109157, 2023.
- [62] Yang M, Huang Z, et al., "Robust object re-identification with coupled noisy labels," *International Journal of Computer Vision*, pp. 1-19, 2024.
- [63] Lin Y, Yang M, Yu J, et al., "Graph matching with bi-level noisy correspondence," in *Proceedings of the IEEE/CVF international conference on computer vision*, 2023, pp. 23362-23371.
- [64] Yang M, Li Y, Hu P, et al., "Robust multi-view clustering with incomplete information," *IEEE Transactions on Pattern Analysis and Machine Intelligence*, vol. 45, no. 1, pp. 1055-1069, 2022.
- [65] C. Szegedy, V. Vanhoucke, S. Ioffe, J. Shlens, and Z. Wojna, "Rethinking the inception architecture for computer vision," in *Proceedings of the IEEE Conference on computer vision and pattern recognition*, 2016, pp. 2818-2826.
- [66] G. Huang, Z. Liu, L. Van Der Maaten, et al., "Densely connected convolutional networks," in *Proceedings of the IEEE conference on computer vision and pattern recognition*, 2017, pp. 4700-4708.
- [67] A. Dosovitskiy, L. Beyer, A. Kolesnikov, et al., "An image is worth 16x16 words: Transformers for image recognition at scale," in *International Conference on Learning Representations*, 2021.
- [68] Danielsson, P. E., "Euclidean distance mapping," *Computer Graphics and image processing*, 14(3), 227-248, 1980.
- [69] J. Shen, Y. Qu, W. Zhang, and Y. Yu, "Wasserstein distance guided representation learning for domain adaptation," in *Proceedings of the AAAI conference on artificial intelligence*, 2018, vol. 32, no. 1.
- [70] Lei B, Zhu Y, Liang E, et al., "Federated Domain Adaptation via Transformer for Multi-site Alzheimer's Disease Diagnosis," *IEEE Transactions on Medical Imaging*, 2023.
- [71] Zhang J, Liu Y, Lei B, et al., "Graph Convolution and Self-attention Enhanced CNN with Domain Adaptation for Multi-site COVID-19 Diagnosis," *45th Annual International Conference of the IEEE Engineering in Medicine & Biology Society*, 2023: 1-4.